EARTHQUAKE ENGINEERING AND STRUCTURAL DYNAMICS
Earthquake Engng Struct. Dyn. 2008; **37**:919–934
Published online 18 February 2008 in Wiley InterScience (www.interscience.wiley.com). DOI: 10.1002/eqe.796

Hysteretic model development and seismic response of unbonded post-tensioned precast CFT segmental bridge columns

Chung-Che Chou*,†,‡ and Chih-Po Hsu§

Department of Civil Engineering, National Chiao Tung University, 1001 Ta-hsueh Rd., Hsinchu 300, Taiwan

SUMMARY

The study investigated the cyclic behavior of unbonded, post-tensioned, precast concrete-filled tube segmental bridge columns by loading each specimen twice. Moreover, a stiffness-degrading flag-shaped (SDFS) hysteretic model was developed based on self-centering and stiffness-degrading behaviors. The proposed model overcomes the deficiency of cyclic behavior prediction using a FS model, which self-centers with fixed elastic and inelastic stiffnesses. Experimental and analytical results showed that (1) deformation capabilities of the column under the first and second cyclic tests were similar; however, energy dissipation capacities significantly differed from each other, and (2) the SDFS model predicted the cyclic response of the column better than the FS model. Inelastic time-history analyses were performed to demonstrate the dynamic response variability of a single-degree-of-freedom (SDOF) system using both models. A parametric study, performed on SDOF systems subjected to eight historical earthquakes, showed that increased displacement ductility demand was significant for structures with a low period and low-to-medium yield strength ratio and reduced displacement ductility demand in these systems was effectively attained by increasing energy dissipation capacity. Copyright © 2008 John Wiley & Sons, Ltd.

Received 21 April 2007; Revised 8 October 2007; Accepted 15 December 2007

KEY WORDS: cyclic test; stiffness-degrading flag-shaped model; time-history analysis

INTRODUCTION

Many studies [1–4] are available on cyclic responses of concrete-filled tube (CFT) columns, which consist of a steel tube filled with concrete. The tube increases compression strength and ultimate strain of confined concrete and contributes to the column's flexural strength. Cyclic response of unbonded, post-tensioned, precast CFT segmental columns has seldom been studied [5–7]. The

*Correspondence to: Chung-Che Chou, Department of Civil Engineering, National Chiao Tung University, 1001 Ta-hsueh Rd., Hsinchu 300, Taiwan.
†E-mail: chchou@mail.nctu.edu.tw
‡Associate Professor.
§Graduate Student Researcher.

behavior of the column subjected to cyclic loading twice is unknown, and no hysteretic model is available for self-centering and stiffness-degrading capabilities.

Hewes and Priestley [8] investigated the seismic behavior of unbonded, post-tensioned, precast concrete segmental bridge columns using the flag-shaped (FS) model, which self-centers with fixed elastic and inelastic stiffnesses. Although the FS model self-centers with energy dissipation characteristics to be modeled explicitly, it does not describe the behavior of strength and stiffness degradation for a column under cyclic loading. Therefore, this study develops a stiffness-degrading flag-shaped (SDFS) model based on cyclic loading experiments of unbonded, post-tensioned, precast CFT segmental bridge columns. The SDFS model self-centers with degradation of strength and stiffness, which are functions of column drift. Time-history analyses, carried out for a single-degree-of-freedom (SDOF) system using both models subjected to eight historical earthquakes, showed a high degree of discrepancy in estimating maximum displacement demand. Owing to the high variability in seismic ground motion, a parametric study was conducted using the SDFS model to determine the effects in terms of displacement ductility demand-of period, yield strength ratio, and energy dissipation capacity on SDOF systems.

OBJECTIVE

The study [9] has the following objectives: (1) investigate experimental behavior of the unbonded, post-tensioned, precast CFT segmental bridge columns under two cyclic loadings, (2) develop an SDFS model based on the hysteretic behavior of the column under cyclic loading, (3) compare seismic responses of an SDOF system using the FS and SDFS models subjected to eight different sets of earthquake data, and (4) determine the effects in terms of displacement ductility demand-of structural characteristics on SDOF systems.

EXPERIMENTAL PROGRAM

Unbonded, post-tensioned, precast CFT segmental column

Two unbonded, post-tensioned, precast CFT segmental columns were designed using the displacement-based approach [10]. To conduct cyclic tests of the columns in the laboratory, the test columns 2450 mm high and 500 mm in diameter were one-sixth of the prototype column. Each test column was composed of a footing, four segments equal in height, and a load stub (Figure 1). The bottom segment was encased in an A36 steel tube with a wall thickness of 5 mm, which was specified to limit extreme fiber-concrete compression strain, as calculated using the confined concrete model [11], to less than $0.5\varepsilon_{cu}$ at 3.5% drift and ultimate strain, ε_{cu}, at 6% drift. The other segments were encased in a 3-mm thick A36 steel tube. Additionally, Specimen 2 included energy-dissipating devices located at the base to increase energy dissipation capacity. The initial post-tensioning forces were 2365 and 2462 kN for Specimens 1 and 2, respectively; the concrete strengths on the day of testing were 53 and 54 MPa for Specimens 1 and 2, respectively. The pre-defined displacement history for the actuator consisted of one drift cycle prior to 0.3%, followed by three drift cycles with amplitudes of 0.4, 0.6, 1.5, 2, 3, 4, 5, and 6%. Detailed information is given in Reference [7].

DOI: 10.1002/eqe

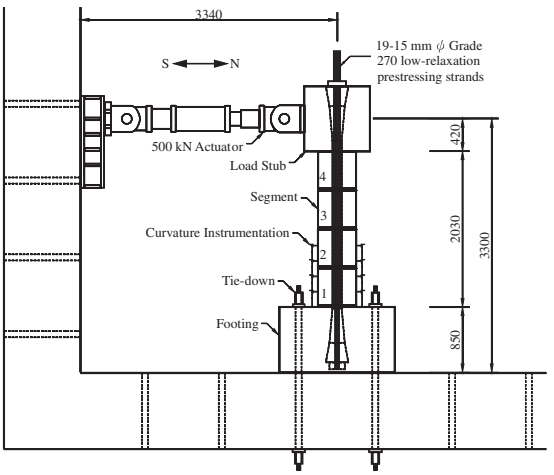

Figure 1. Test setup (Specimen 1).

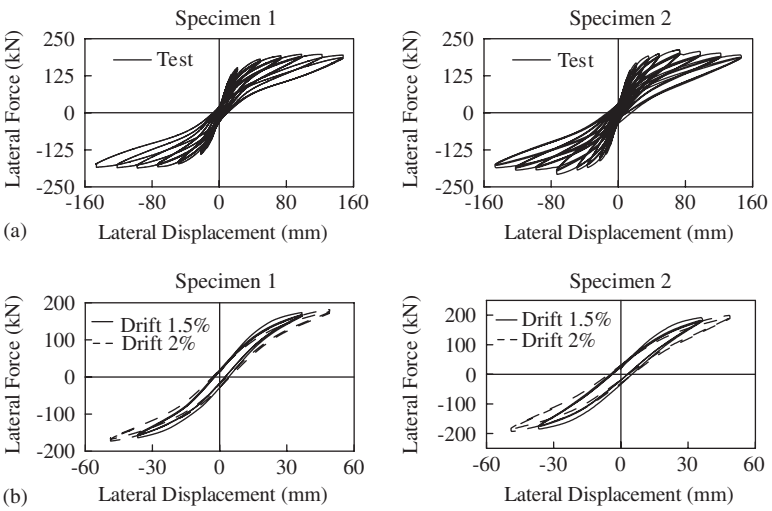

Figure 2. Column lateral force–displacement relationship (first test): (a) full response and (b) 1.5% and 2% responses.

Experimental response

Figure 2(a) shows hysteretic responses of two specimens under the first cyclic loading to a 6% drift (147 mm). The area within the hysteresis loop is accumulated energy dissipation, which is larger in Specimen 2 due to the energy-dissipating devices placed at its base. Figure 2(b) shows hysteretic loops with drift amplitudes of only 1.5% (37 mm) and 2% (49 mm). For a specific displacement amplitude, the lateral force in the first cycle is always larger than that in subsequent cycles. The lateral force–displacement relationship in the first cycle of loading to a new and higher drift level

DOI: 10.1002/eqe

follows that in the third cycle of a previous drift. This behavior occurs because the concrete at the column base was damaged by loading during the first cycle, reducing the lateral strength in subsequent cycles. Minor concrete spalling at the interface between segments 1 and 2 and concrete crushing at the column base were observed after the tests for both specimens, leading to a slight strength reduction [7].

Since the column damage was concentrated at the base (Figure 3(a)), the crushed concrete was removed and the gap was filled with epoxy. The initial post-tensioning force in Specimen 2 increased to 3160 kN; no energy-dissipating devices were provided at the column base. Two retrofitted specimens were retested under the same displacement cycles; the hysteretic response (Figure 4) shows much less energy dissipation compared with that in the first test (Figure 2(a)). Figure 5 shows the relationship between stiffness and drift obtained from the column lateral force–displacement relationship, from which elastic stiffness was evaluated at each drift using experimental data between the two steps. The first step represents the location of the hysteretic response when column displacement reaches zero. The second step represents the location of the hysteretic response when the column base crack reaches mid-depth of the column section. Inelastic stiffness was evaluated using experimental data between the second step and peak strength at the first cycle of each drift. In the first test, elastic stiffness of Specimens 1 and 2 decreased from 9.3

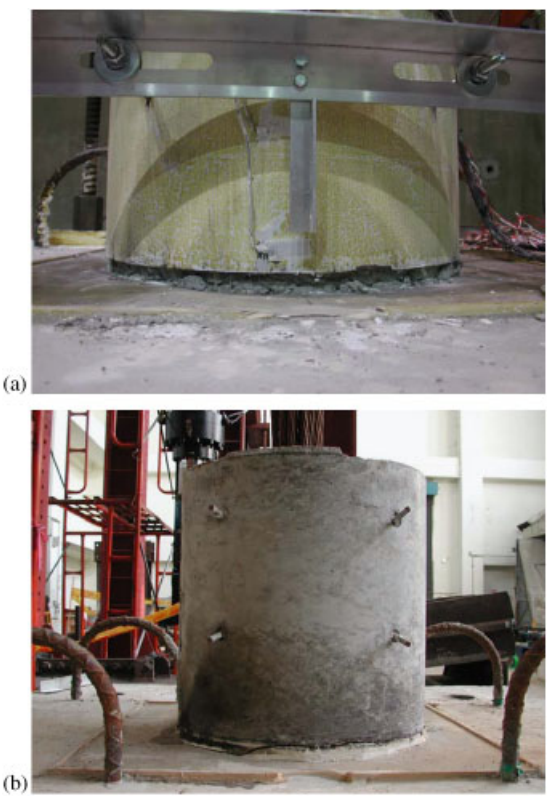

Figure 3. Concrete damage in the first segment (Specimen 1): (a) first test (6% drift) and (b) second test (after test).

DOI: 10.1002/eqe

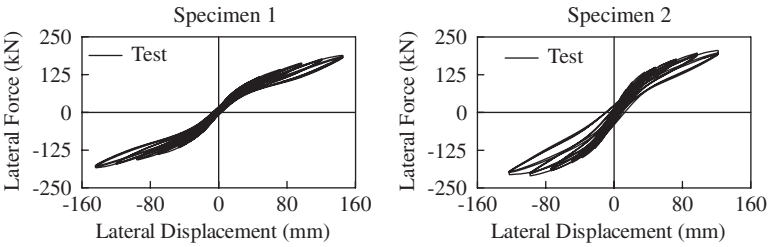

Figure 4. Column lateral force–displacement relationship (second test).

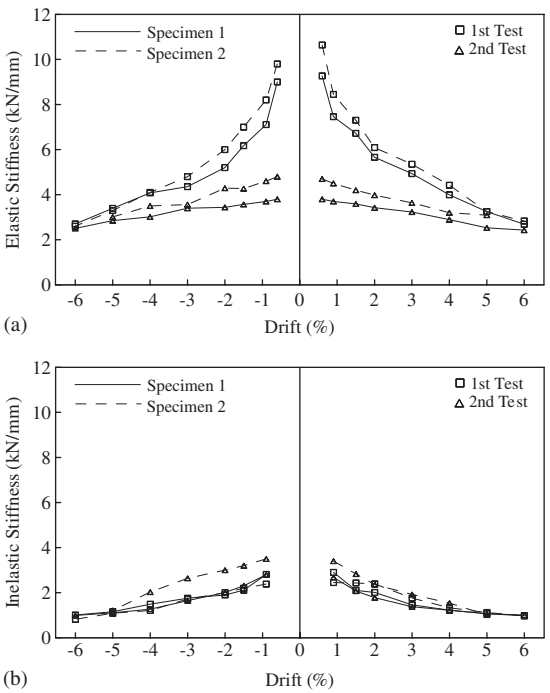

Figure 5. Stiffness *versus* drift relationship: (a) elastic stiffness *versus* drift and (b) inelastic stiffness *versus* drift.

to 2.7 kN/mm and from 10.6 to 2.8 kN/mm, respectively, at a drift of 6% (Figure 5(a)), resulting in a reduction in stiffness of about 70%. The inelastic stiffness of Specimens 1 and 2 decreased from 3.5 and 3.9 kN/mm to about 1 kN/mm (Figure 5(b)), resulting in a reduction in stiffness of 65 and 74%, respectively.

The steel jacket was removed from the first segment after the second test for examining concrete damage. Figure 3(b) shows that minor diagonal cracks occurred in the concrete segment and split cracks occurred at the retrofitted base. The epoxy failure at the base did not exhibit gradual crush behavior as observed for concrete failure in the first test. Stiffness degradation was, therefore,

DOI: 10.1002/eqe

less severe in the second test than in the first test. Furthermore, hysteretic energy dissipation was associated with the plastic straining of concrete in compression, but the epoxy at the retrofitted base exhibited elastic responses, leading to a significant reduction in energy dissipation for the second test.

HYSTERETIC MODELS

Flag-shaped model

Hewes and Priestley [8] utilized the FS model to investigate the seismic response of unbonded, post-tensioned, concrete segmental bridge columns. Figure 6(a) shows the idealized column lateral force–displacement relationship of the FS model, which follows bilinear-elastic rules with hysteretic energy added to the post-elastic portion of response, leading to self-centering with fixed elastic and inelastic stiffnesses. An independent response parameter α reflects energy dissipation capacity. Table I lists modeling parameters: initial elastic stiffness K_e, inelastic stiffness K_p, yield

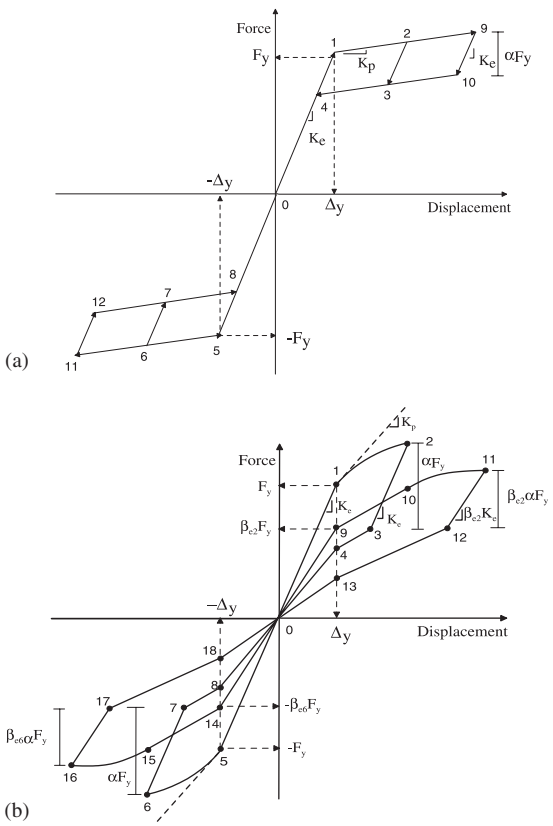

Figure 6. Idealized column lateral force–displacement relationship for (a) FS and (b) SDFS models.

DOI: 10.1002/eqe

Table I. Parameters in predicting cyclic response of specimens.

Model	Specimen no.	K_e (kN/mm)	K_p (kN/mm)	Δ_y (mm)	α
(a) First test					
FS	1	9.3	0.4	17.9	0.33
	2	10.5	0.6	16	0.45
SDFS	1	9.3	3.5	12.2	0.46
	2	10.5	3.9	12.2	0.52
(b) Second test					
FS	1	3.8	1.01	17.9	0.45
	2	4.7	1.08	16	0.46
SDFS	1	3.8	2.7	10	0.5
	2	4.7	3.4	12.7	0.6

displacement Δ_y, and parameter α. Elastic stiffness and inelastic stiffness were determined according to the work by Hewes and Priestley [8]. Yield displacement of the FS model was determined by the lateral force, three times the decompression force, divided by the elastic stiffness [8]. The average value of α, each of which was determined by equating hysteretic energies calculated from the test specimen and the FS model at each drift, was used in prediction.

Stiffness-degrading flag-shaped model

Figure 6(b) shows the idealized column lateral force–displacement relationship in the SDFS model. Before the crack at the column base reaches mid-depth of the section, the column lateral force–displacement response shows elastic behavior with initial elastic stiffness K_e. The crack propagating to mid-depth of the column section represents the beginning of a nonlinear response (step 1). The initial inelastic stiffness K_p is determined as a slope between step 1 and the location when extreme concrete-fiber strain at the column base reaches 0.004. This strain level is often assumed as threshold for spalling of unconfined concrete [10]. Associated with this hysteretic model are three independent response parameters α, β_{ei}, and β_{pi}. Parameter α, similar to that in the FS model, represents energy dissipation capacity. Stiffness-degrading parameters, β_{ei} and β_{pi}, are functions of a column displacement ratio (Δ/Δ_y) and are expressed as

$$\beta_{ei} = \frac{K_{ei}}{K_e} \tag{1}$$

$$\beta_{pi} = \frac{K_{pi}}{K_p} \tag{2}$$

where K_{ei} and K_{pi} are the elastic and inelastic stiffnesses at the ith drift. Figure 7(a) shows the relationship between β_{ei}, β_{pi}, and the displacement ratio for both specimens under the first cyclic test. Δ_y is the yield displacement when the column base crack reaches mid-depth of the section, and Δ is the column displacement at a specified drift. Figure 7(b) shows parameters for both specimens under the second cyclic test; elastic stiffness degradation in the second test is not as significant as that in the first test.

DOI: 10.1002/eqe

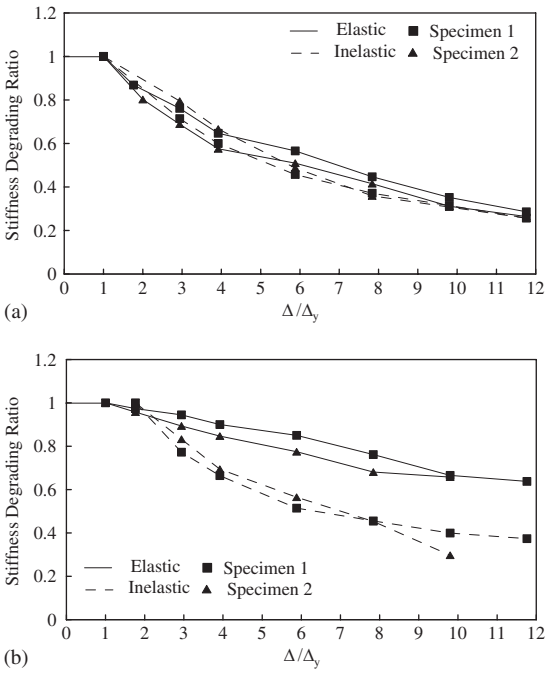

Figure 7. Stiffness degradation *versus* displacement ratio: (a) first test and (b) second test.

Under continued loading, yielding begins at step 1. The model becomes nonlinear and exhibits varying stiffness with increasing displacement. The corresponding force F_2 is given by

$$F_2 = F_y + \sum_{i=1}^{n} \overline{K}_{pi} \overline{d}_{pi} \tag{3}$$

where F_y is the yield force; n is the number of increment from steps 1 to 2, and $\overline{d}_{pi}$ is the displacement increment, in which a constant inelastic stiffness $\overline{K}_{pi}$, which is a function of the displacement ratio and data (Figure 7), is assumed. Upon reversal of loading at step 2, the model exhibits linear elastic behavior until a reduction in lateral force, αF_y, is reached at step 3. The corresponding displacement at that point is given by

$$\Delta_3 = \Delta_2 - \frac{\alpha F_y}{K_e} \tag{4}$$

The inelastic stiffness between steps 3 and 4 is the average inelastic stiffness from steps 1 to 2, identified as $K_{p1,2}$. After the model reaches the yield displacement at step 4, it self-centers without producing residual displacement. At step 4, the lateral force is given by

$$F_4 = (F_2 - \alpha F_y) - (\Delta_3 - \Delta_y) K_{p1,2} \tag{5}$$

If the model is reloaded while unloading between steps 3 and 4, the model exhibits the elastic stiffness, K_e, until reaching a point in a line drawn from steps 1 to 2, followed by the inelastic stiffness, $K_{p1,2}$. If the model is reloaded while unloading between step 4 and the origin, the

DOI: 10.1002/eqe

model also exhibits the elastic stiffness, K_e, until reaching the yield displacement, followed by the inelastic stiffness, $K_{p1,2}$. The model has been developed assuming that stiffness degradation is mobilized once unloading continues until the origin has been reached. A symmetric response is obtained when the load is applied in the opposite direction.

Upon reloading from the origin to step 9, the elastic stiffness is $\beta_{e2}K_e$, where parameter β_{e2} is calculated based on displacement Δ at step 2, yield displacement Δ_y, and relationship between stiffness degradation and displacement ratio (Figure 7). The yield force decreases from F_y to $\beta_{e2}F_y$ due to a fixed yield displacement. Before the model reaches step 10, which has the same displacement as that at step 2, the inelastic stiffness is always $\beta_{p2}K_p$, where parameter β_{p2} is calculated based on displacement Δ at step 2, yield displacement Δ_y, and relationship between stiffness degradation and displacement ratio (Figure 7). The inelastic stiffness starts degrading after the model displacement passes step 10, leading to a varying inelastic stiffness from steps 10 to 11. When the loading direction is reversed at step 11, the model exhibits a linear elastic stiffness until the force reduction of $\beta_{e2}\alpha F_y$ is reached. Small force reduction is due to the small yield force in this reloading cycle. The inelastic stiffness between steps 12 and 13 is the average inelastic stiffness between steps 9 and 11, denoted as $K_{p9,11}$. If the model is reloaded while unloading between steps 12 and 13 or between step 13 and the origin, the model follows the previous reloading rule with an updated elastic stiffness, $\beta_{e2}K_e$, and inelastic stiffness, $K_{p9,11}$. Table I lists the initial elastic stiffness K_e, inelastic stiffness K_p, yield displacement Δ_y, and parameter α to predict the cyclic responses of test specimens. Because the yield displacement of the SDFS model corresponds to the stage when the crack at the column base has propagated to mid-depth of the section, the yield displacement is smaller in the SDFS model than in the FS model. The average value of α, each of which was determined by equating hysteretic energies calculated from the test specimen and the SDFS model at each drift, was used in prediction.

Prediction comparison between FS and SDFS models

Figures 8 and 9 show the cyclic responses of the unbonded, post-tensioned, precast CFT segmental bridge column using the FS and SDFS models, respectively. Only the SDFS model shows that the lateral force in the first cycle is higher than that in the other cycles at any specific drift, and that the column lateral force–displacement relationship in the first cycle follows that in the third cycle of a previous drift. There is a satisfactory similarity between the test response and SDFS model prediction in estimating elastic and inelastic stiffnesses at each drift (Figure 10). However, the FS model always has fixed elastic and inelastic stiffnesses throughout the displacement cycles. The energy dissipation obtained from specimen tests can be modeled well for both models (Figure 11). Note that the hysteretic energies predicted by both models for Specimen 2 are larger than those from the test after a 3% drift because fractures of energy dissipation devices [7] are not modeled. Lateral forces predicted by both models in Figures 8 and 9 are, therefore, larger than those from Specimen 2 test.

DYNAMIC ANALYSES OF SDOF SYSTEMS

Time-history analysis

Hysteretic behavior of the SDOF system was characterized by the unbonded, post-tensioned, precast CFT segmental column. Because the prototype column was 6 times its scaled test column, the

DOI: 10.1002/eqe

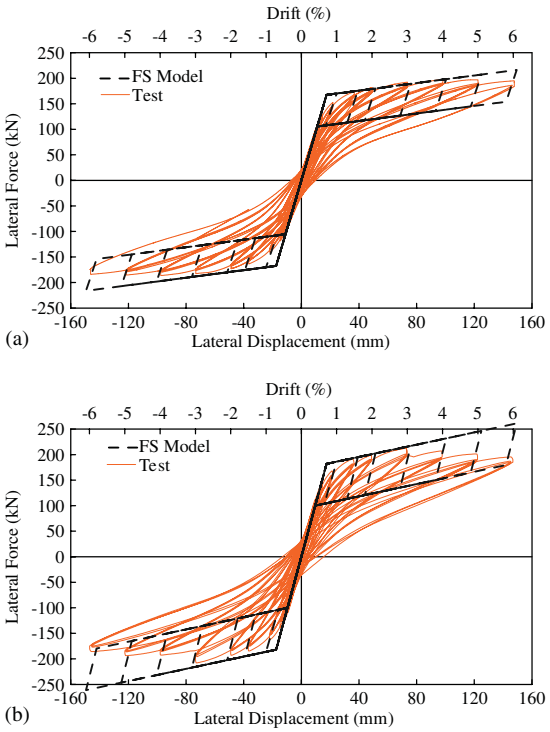

Figure 8. Prediction based on FS Model (first test): (a) Specimen 1 and (b) Specimen 2.

elastic stiffness, inelastic stiffness, and yield displacement of the prototype column were calculated based on the scaling factor and parameters in both models (Table I(a)) in predicting Specimen 1 response. The relationship between stiffness degradation and displacement ratio (Figure 7(a)) was used for the SDFS model. The elastic damping ratio of 0.05, which was proportional to the initial stiffness, was used for analyses. The SDOF system had the fundamental period 1.26 s and was excited by each of the eight different earthquakes to examine seismic performance.

These records from California and Taiwan were free of any forward directivity effects (near-field effects). All records were recorded for soil type C and were generated by earthquakes of moment magnitude ranging from 6.7 to 7.3. Since the prototype column was designed for $0.7g$ maximum ground motion acceleration on soil type C, 5% damped-design elastic acceleration and displacement response spectra taken directly from the ATC-32 document [12] were constructed and used as the target spectra. Each of the eight earthquake records was scaled to minimize the square of error between its 5% damped response spectrum and target spectrum. Table II lists scaled peak ground accelerations for each record, and Figure 12 presents each of the eight scaled records along with the ATC 32 target spectra. A good match exists between mean spectra values and the target spectrum.

Figure 13 shows the seismic response of the SDOF system for the FS and SDFS models. Although the FS and SDFS models possess self-centering and energy dissipation capabilities, no degradations of stiffness and strength are included in the FS model, resulting in different seismic

DOI: 10.1002/eqe

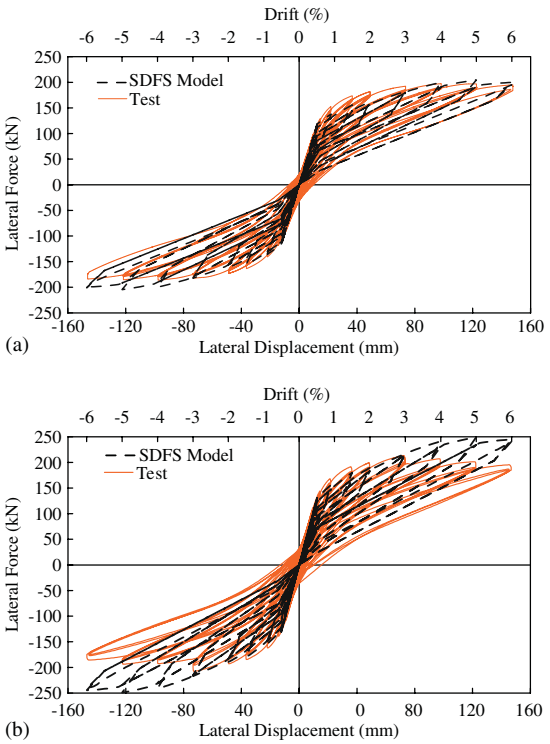

Figure 9. Prediction based on SDFS model (first test): (a) Specimen 1 and (b) Specimen 2.

responses. Table II also lists the maximum displacement of the SDOF system for both models; the prediction discrepancy ranges from 88 to 209%, indicating the effects of stiffness degradation on dynamic response of unbonded, post-tensioned, precast CFT columns.

Parametric study

The parametric study presented herein focuses only on the seismic response of the SDOF system using the SDFS model. The two key parameters used for defining dynamic response of the SDOF system are initial period T_e and yield strength ratio C_y:

$$T_e = 2\pi\sqrt{m/k_e} \tag{6}$$

$$C_y = F_y/mg \tag{7}$$

where K_e is the initial elastic stiffness of the system; F_y is the initial yield force; m is the mass; and g is gravity acceleration. Moreover, the SDFS model uses parameter specification of Specimen 1 (Figure 7(a)) for energy dissipation, and degradation of elastic and inelastic stiffnesses. Table III lists the complete sets of parameters T_e, C_y, and α considered. The first value of $\alpha = 0.46$ is similar

DOI: 10.1002/eqe

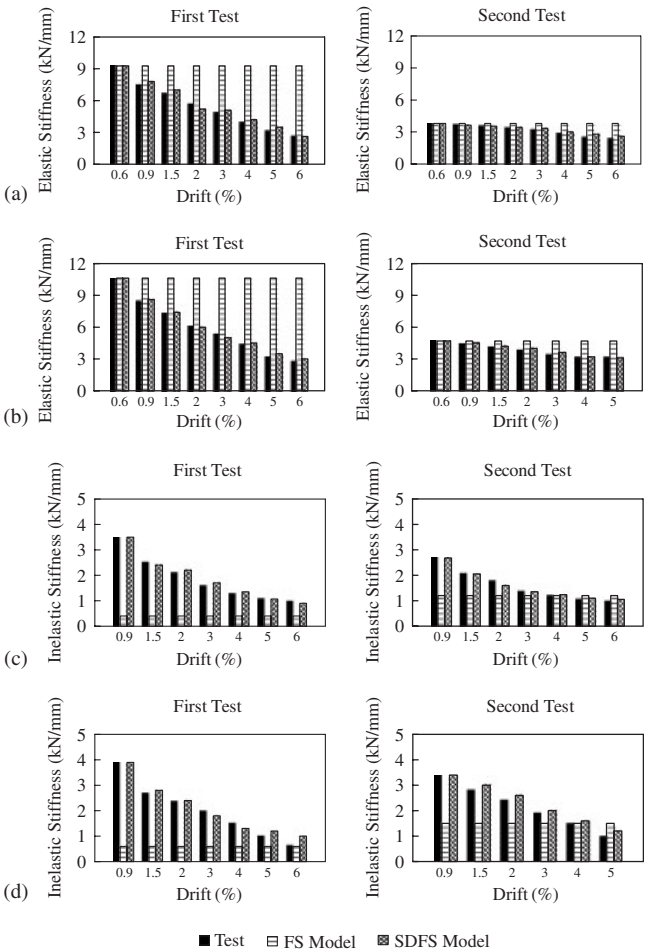

Figure 10. Elastic and inelastic stiffness predictions *versus* test results: (a) Specimen 1 (elastic stiffness); (b) Specimen 2 (elastic stiffness); (c) Specimen 1 (inelastic stiffness); and (d) Specimen 2 (inelastic stiffness).

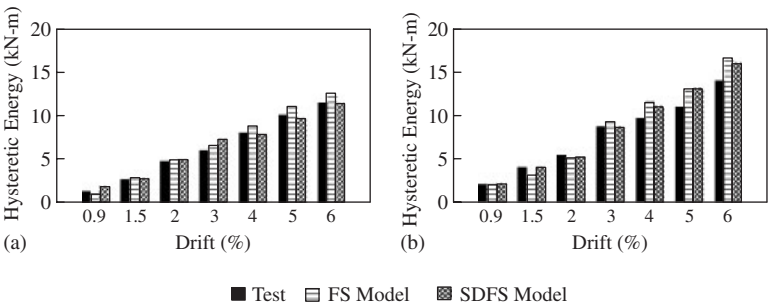

Figure 11. Hysteretic energy prediction *versus* test results (first test): (a) Specimen 1 and (b) Specimen 2.

DOI: 10.1002/eqe

Table II. Characteristics of earthquake records.

Earthquake event	Year	Station	PGA (g)	Scaled PGA (g)	Distance (km)	Displacement (mm)	
						FS model	SDFS model
Loma Prieta	1989	1652 Anderson Dam (downstream)	0.24	0.86	21	274	131
		58065 Saratoga-Aloha Ave.	0.32	0.96	13	587	443
Landers	1992	22170 Joshua Tree	0.28	0.73	11	525	439
		Coolwater	0.42	0.92	21	172	360
Northridge	1994	90013 Beverly Hills-14145 Mulhol	0.52	0.93	20	418	476
		24278 Castsic-Old Ridge Route	0.51	0.66	21	300	245
Chi-Chi	1999	TCU034	0.25	0.57	33	120	92
		TCU039	0.21	0.73	17	936	968

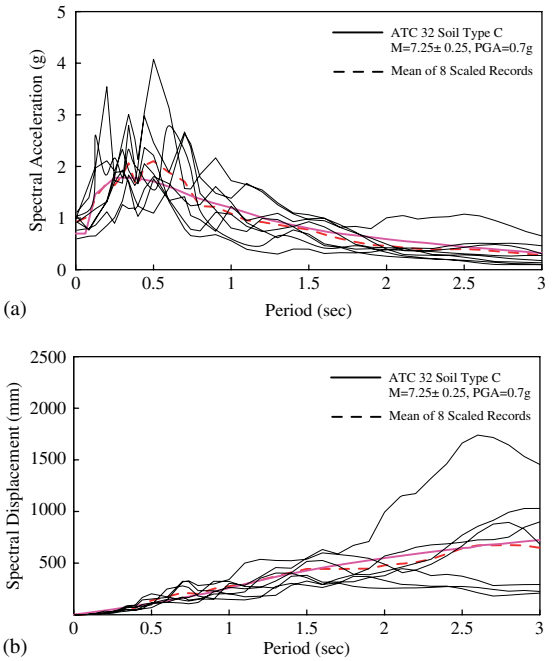

Figure 12. Elastic response spectra of ATC-32 and eight scaled records: (a) elastic acceleration response spectra and (b) elastic displacement response spectra.

to that calculated based on experimental results. The use of $\alpha = 0.92$ illustrates the effects by increasing energy dissipation of the system in reducing maximum displacement demand. Each SDOF system was subjected to eight different scaled ground motions to estimate seismic demands; thus, a total of 640 SDOF time-history analyses were carried out.

DOI: 10.1002/eqe

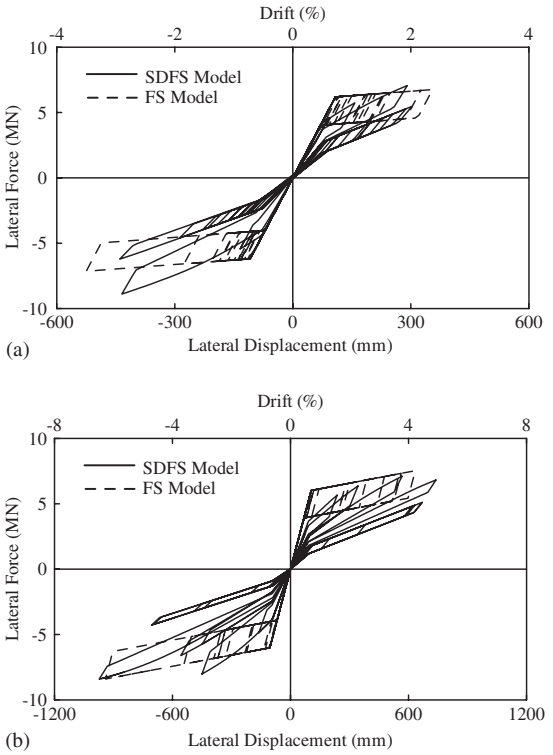

Figure 13. Comparison between SDFS and FS models subjected to earthquakes: (a) landers: Joshua tree and (b) Chi-Chi: Tcu039.

Figure 14 shows the mean values over the set of earthquakes of maximum displacement and displacement ductility demands. The maximum displacement demand generally increases for increasing values of initial period T_e. When α increases, the reduction in maximum displacement demand is more significant for $C_y = 0.1$ than for other C_y values. Mean displacement ductility demand is reduced in all cases for increasing values of α, particularly for $C_y = 0.1$. An increase in displacement ductility demand is most significant for structures with low period ($T_e \leqslant 1.0$ s) and low-to-medium yield strength ratio ($0.1 \leqslant C_y \leqslant 0.5$). The trends observed in these analyses are similar to those previously observed for other hysteretic models describing the dynamic response of reinforced concrete members [13, 14].

CONCLUSIONS

Two unbonded, post-tensioned, precast CFT segmental bridge columns were tested twice under cyclic loading to evaluate seismic response. For the column subjected to the first cyclic loading, the lateral force in the first cycle was always higher than that for other cycles at each drift. This behavior occurred because the concrete at the column base was damaged by loading during the first cycle, reducing the lateral strength in subsequent cycles. The reduction in elastic and inelastic

DOI: 10.1002/eqe

Table III. Parameters of T_e, C_y, and α considered in the study.

T_e (s)	0.1	0.25	0.5	1.0	1.5	2.0	2.5	3.0
C_y	0.1	0.2	0.4	0.5	0.8	—	—	—
α	0.46	0.92	—	—	—	—	—	—

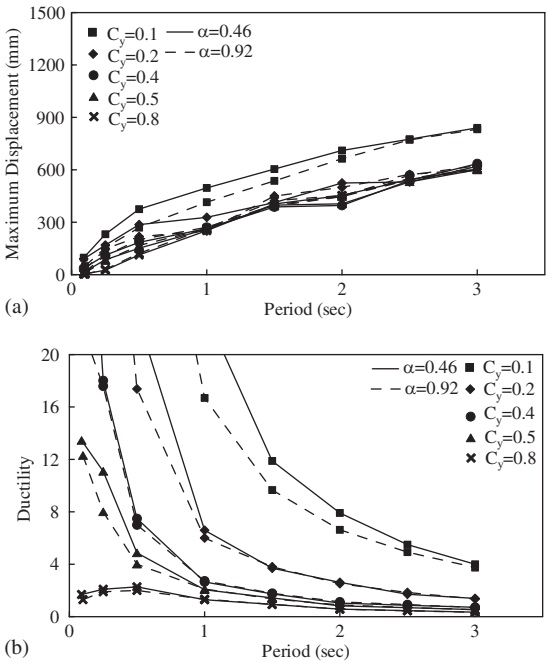

Figure 14. (a) Maximum displacement and (b) ductility demand response spectra.

stiffnesses was about 70% at a drift of 6%. For the column subjected to the second test, the area enclosed by hysteretic loops was significantly smaller than that during the first test, indicating small energy dissipation. However, reduction in elastic stiffness was not as significant as that during the first test because the epoxy for retrofitting the base did not show gradual crush failure as observed for the original concrete base.

Although the FS model follows bilinear-elastic rules with hysteretic energy added to the post-elastic portion of the response, it cannot predict degradation of stiffness and strength of the unbonded, post-tensioned, precast CFT segmental bridge columns under testing. The SDFS model, developed based on experiments, has three parameters for considering the effects of energy dissipation and stiffness degradation of the columns. Detailed comparisons between test responses and both models showed that although hysteretic energies predicted by both models were close to those obtained from the column tests, the general hysteretic behaviors of the columns were reasonably predicted by using the SDFS model rather than the FS model. Time-history analyses performed on SDOF systems using both models further demonstrated the variability of maximum

DOI: 10.1002/eqe

displacement. The prediction discrepancy from both models ranged from 88 to 209%, indicating that both energy dissipation and stiffness degradation are key parameters in predicting dynamic responses of unbonded, post-tensioned, precast CFT columns.

A parametric study was conducted to determine the effect of period, yield strength ratio, and energy dissipation of SDOF systems in terms of displacement ductility demand. The increase in displacement ductility demand was most significant for structures with a low period ($T_e \leqslant 1.0$ s) and low-to-medium yield strength ratio ($0.1 \leqslant C_y \leqslant 0.5$), and the reduced displacement ductility demand in these systems was effectively achieved by increasing energy dissipation capacity.

Although the SDFS model could predict the cyclic responses of test specimens, more unbonded, post-tensioned, precast concrete column tests, emphasizing on stiffness reduction associated with different concrete confinements or cross-sectional shapes, are needed to increase the database. Thus, the parameters of the SDFS model could be developed as a general approximation for practical uses.

ACKNOWLEDGEMENTS

Financial support for this study was provided by the National Chiao Tung University, Taiwan.

REFERENCES

1. Usami T, Ge H. Ductility of concrete-filled steel box columns under cyclic loading. *Journal of Structural Engineering* (ASCE) 1994; **120**(7):2021–2040.
2. Susantha KAS, Ge H, Usami T. Cyclic analysis and capacity prediction of concrete steel box columns. *Earthquake Engineering and Structural Dynamics* 2002; **31**:195–216.
3. Boyd PF, Cofer WF, McLean DI. Seismic performance of steel-encased concrete column under flexural loading. *ACI Structures Journal* 1995; **92**:355–364.
4. Elremaily A, Azizinamini A. Behavior and strength of circular concrete-filled tube columns. *Journal of Constructional Steel Research* 2002; **58**:1567–1591.
5. Billington SL, Barnes RW, Breen JE. A precast segmental substructure system for standard bridges. *PCI Journal* 1999; **44**(4):56–73.
6. Hewes JT, Priestley MJN. Seismic design and performance of precast concrete segmental bridge columns. *Report No. SSRP 2001/25*, University of California, San Diego, La Jolla, CA, 2002.
7. Chou C-C, Chen Y-C. Cyclic tests of post-tensioned precast CFT segmental bridge columns with unbonded strands. *Earthquake Engineering and Structural Dynamics* 2006; **35**:159–175.
8. Hewes JT. Seismic design and performance of precast concrete segmental bridge columns. *Doctor Thesis*, Priestley MJN (advisor), University of California, San Diego, CA, 2002.
9. Hsu C-P. Hysteretic model and seismic response of post-tensioned segmental bridge columns. *Master Thesis*, Chou C-C (advisor), National Chiao Tung University, Hsinchu, Taiwan, 2006.
10. Priestley MJN, Seible F, Calvi GM. *Seismic Design and Retrofit of Bridges*. Wiley: New York, 1996.
11. Mander JB, Priestley MJN, Park P. Theoretical stress–strain model for reinforced concrete. *Journal of Structural Engineering* (ASCE) 1988; **114**(8):1804–1823.
12. ATC 32. Improved seismic design criteria for california bridges: provisional recommendations. *Report No. ATC-32*, Applied Technology Council, Redwood City, CA, 1996.
13. Saiidi M, Sozen MA. Simple and complex models for nonlinear seismic response of reinforced concrete structures. *Structural Research No. 465*, Civil Engineering Studies, University of Illinois at Urbana-Champaign, Urbana, 1979.
14. Otani S. Hysteresis models of reinforced concrete for earthquake response analysis. *Journal of Faculty of Engineering* 1981; **VI**(2):125–159.

DOI: 10.1002/eqe